Schweizerische Eidgenossenschaft
Confédération suisse
Confederazione Svizzera
Confederaziun svizra

Eidgenössisches Departement für
Umwelt, Verkehr, Energie und Kommunikation UVEK

Bundesamt für Energie BFE

TOM

ERSTELLUNG EINES THERMOELEKTRISCHEN OXIDISCHEN MODULS (TOM) ALS DEMONSTRATOR

Jahresbericht 2008

Autor und Koautoren	Petr Tomeš and Anke Weidenkaff
beauftragte Institution	Empa
Adresse	Ueberlandstrasse 129 CH-8600 Duebendorf, Switzerland
Telefon, E-mail, Internetadresse	+41 44 823 41 31, anke.weidenkaff@empa.ch
BFE Projekt-/Vertrag-Nummer	101356/152820
BFE-Projektleiter	Anke Weidenkaff
Dauer des Projekts (von – bis)	
Datum	28.11.2008

ZUSAMMENFASSUNG

Novel recently discovered non-conventional thermoelectric oxides were produced and characterised to verify their thermoelectric conversion potential. Four - leg thermoelectric oxide modules (TOM) were fabricated by combining *p*- and *n*-type oxide thermoelements made of pressed polycrystalline $GdCo_{0.95}Ni_{0.05}O_3$ [1] and $CaMn_{0.98}Nb_{0.02}O_3$ [2], respectively.

By using the High – Flux Solar Simulator (HFSS) at ETH as source of simulated solar radiation it was demonstrated that the direct conversion of solar heat into electrical energy can be achieved with the TOM. The temperature difference (ΔT) between the hot and the cold side of the module was tuned by using different arc electrical input current supplied by an argon arc. The maximum output power of 0.032 W was reached for ΔT = 450 K. The maximum conversion efficiency of ~ 1 % was achieved using an arc current of 200 A which induced a maximum ΔT of 470 K in the TOM.

Projektziele

Thermoelectric materials are candidates for the devices, which can directly convert heat into electrical energy. The energy conversion efficiency of thermoelectric materials has to be improved by enhancing the thermoelectric figure of merit, Z, defined as $Z = \sigma S^2 \kappa^{-1}$ (σ is the electrical conductivity, S is the Seebeck coefficient and κ is the thermal conductivity) of the thermoelectrics. At Empa new promising unconventional materials are developed and tested in thermoelectric applications. The choice, assembly and demonstration of te thermoelectric conversion is the main goal of the TOM project. Strongly electron correlated systems of ruthenates and misfit cobaltates are interesting because the electronic structure is influenced not only by charge, but also by the spin, lattice and orbital degrees of freedom.

Durchgeführte Arbeiten und erreichte Ergebnisse

1) Thermoelectric oxide module (TOM) – generating electricity from solar radiation

Four leg thermoelectric modules made of thermoelectric materials developed and produced at Empa were assembled to be characterised in a dedicated test stand for further use as solar energy converters.

The High – Flux Solar Simulator HFSS at the Institute of Energy Technology, ETH, Zürich (Figure 1a) is able to supply flux intensity above 500 W/cm^2 and process temperatures exceeding 3000 K. The HFSS is cooled by water which flows between the argon arc and the quartz lamp tube. The arc produces radiation at visible wavelengths with additional part of the spectrum in the infrared and ultraviolet regions. Power flux intensity and temperature can be adjusted by varying the position of the target along the axis of the focusing mirrors or by changing the electrical input power given to the arc electrodes.

By placing the TOM in the focus the heat supplied by the HFSS was converted into electricity. The TOM was coated on the hot side by homogeneous black graphite layer (see Figure 1b) to increase the absorption of solar radiation by improving the emissivity value of the hot side of the module.

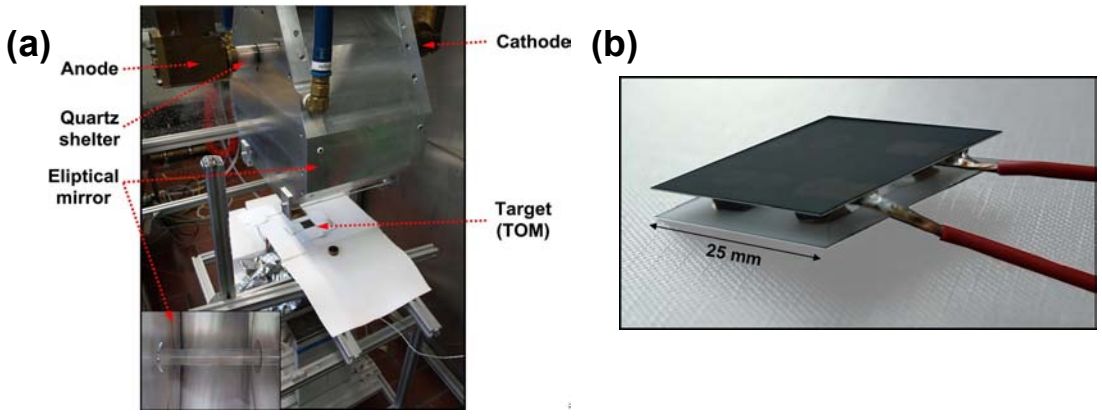

Figure 1: (a) The High-Flux Solar Simulator at ETH with the enclosed argon arc lamp by an elliptical mirror that redirects the radiant power into the target (TOM) and (b) photo of a four - leg thermoelectric oxide module with a coated graphite layer on the hot side.

The output power measurements were done by applying different electrical input current (50, 100, 150 and 200 A) to the arc electrodes. In each measurement, an electrical input current was applied, when the temperature was stable, and a power output was measured. The maximum temperature difference by applying an arc current of 200 A was ΔT = 470 K. The temperature evolution on the

hot and the cold side of the TOM when increasing the intensity of the arc current is plotted in Figure 2a. Four temperatures were stabilised (see the bar areas in Figure 2a). The output power as a function of the voltage was measured for different ΔT (see Figure 2b).

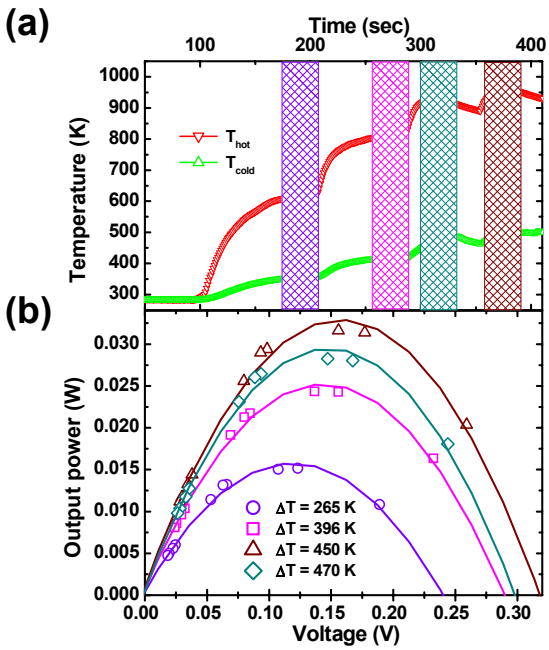

Figure 2:.(a) Time evolution of the temperature at hot side and cold side of the module measured by the K-type thermocouples and (b) output power vs. voltage for different ΔT.

The output power increases with increasing temperature gradient of the TOM. For the electrical current of 200 A which induced ΔT = 470 K, the output power decreased. This was caused by the formation of substantial cracks across the *p*-type leg of the module which caused the increase of total internal resistance of the TOM. The main reasons for crack formations across the *p*-type leg are probably the higher value of the thermal expansion coefficient of the *p*-type leg (α ~ 26.5 K^{-1}) compared to the Al_2O_3 (α ~ 8.0 K^{-1}) and the speed of the heating. In 4.5 min the temperature on the hot side increased up to 965 K which could induce a thermal “shock” to the material. The ΔT between the hot side and the cold side for the arc current 200 A increased only ~ 20 K more because of the insufficient cooling.

The maximum output power was calculated from the output power curves in Figure 2b considering the load resistance equal to the internal resistance and is plotted in Figure 3a. The maximum output power is increasing with increasing ΔT up to ΔT = 450 K. For ΔT = 470 K the maximum output power decreased (see the red frame in Figure 3a). The reason for this unusual behaviour was described previously.

The conversion efficiency of a four – leg TOM with the cross – section of the leg 4 x 4 mm^2 (see Figure 3b) was calculated from the evaluation of the *ZT* values of the *p*- and *n*-type materials and the measurements of the temperature on the hot and cold side of the module. If we calculate the conversion efficiency using the formula [3]:

$$\eta = \frac{T_h - T_c}{T_h} \frac{\sqrt{1 + Z\left(\frac{T_h + T_c}{2}\right)} - 1}{\sqrt{1 + Z\left(\frac{T_h + T_c}{2}\right)} + \frac{T_c}{T_h}}, \quad (1)$$

where T_c and T_h are temperature on the cold and hot side, respectively and Z is the Figure of Merit of the *p*- and *n*-type material, we obtain a maximum conversion efficiency of ~ 1 % at ΔT = 470 K.

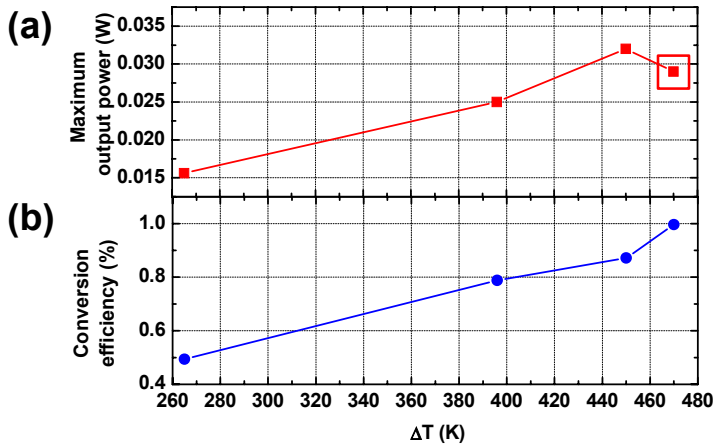

Figure 3: (a) Maximum output power and (b) conversion efficiency as function of ΔT.

2) Development of materials with strongly electron correlated systems

a. $Na_{1-x}Sr_xRuO_3$

$SrRuO_3$ is a metallic – like ferromagnet with a relatively high Curie temperature (T_C ~ 160 K) [4]. Perovskite-type $SrRuO_3$ belongs to the ”class of strongly electron correlated systems” because of the synergy of the transport and magnetic properties. However, the ferromagnetism of $SrRuO_3$ is of the itinerant type at least in a sense that the magnetization does not reach the theoretical limit S = 1 (2 μ_B / Ru); surprisingly the $CaRuO_3$ compound despite the same crystal structure, high metallicity and similar magnetic response at high temperatures remains paramagnetic down to lowest temperatures. These different physical properties have been attributed to the difference in lattice distortion and / or the A cation influence on the 4*d* Ru bands widths and, hence, on the relative populations of the spin-up and spin-down bands. To study these effects in detail we have prepared by solid state reaction synthesis $SrRuO_3$ where the Sr were substituted by single valent Na ions; the role of substituent was then both in the modification of the crystal structure but, more importantly, in the possibility to influence the filling of 4 *d* Ru orbital via the charge compensation.

The polycrystalline ceramic samples of $Sr_{1-x}Na_xRuO_3$ (x = 0.0, 0.10, 0.20 and 0.25) were prepared by solid - state reaction method. Stoichiometric amounts of $SrCO_3$ (99.9+%), Na_2CO_3 (99.9+%) and RuO_2 (99.9+%) were mixed, homogenized in agate mortar and calcinated at 873 K in air for 24 h. After calcination the final powder had been reground and pressed into pellets, final sintering was performed at 1323 K for 40 h in air followed by slow cooling to avoid the oxygen nonstochiometry.

All the compounds of the $Sr_{1-x}Na_xRuO_3$ system have orthorhombic crystal structure with *Pbnm* space group. In Figure 4 is plotted the composition dependence of lattice parameters together with the composition dependence of the unit cell volume which is displayed in the inset of Figure 1a. The relation $a > c/\sqrt{2} > b$ is valid for all the range of Na doped compounds. The unit cell volume is decreasing over all the range of compositions. The lattice parameters are monotonously decreasing with increasing of Na content. From the Rietveld refinement was found that the real Na content of the samples are 8, 14 and 18 % instead of 10, 20 and 25 %. If we consider this lower Na content the descending trend of the lattice parameters and unit cell volume will be more linear. In Figure 4 is also plotted the orthorhombic distortion vs. A ionic radius (A = Sr, Na), which is defined in Ref. [5]. $SrRuO_3$ has almost ideal

perovskite cubic structure with a small orthorhombic distortion. The orthorhombic distortion for $Sr_{1-x}Na_xRuO_3$ (x = 0.0 - 0.25) is in the range of 0.384 % up to 0.443 %.

The evolution of Ru – O bond distances and Ru – O – Ru bond angles are displayed in Figure 4b. The Ru – O bond evolution is slightly decreasing with increasing of the Na content. The Ru – O – Ru bond angle has descending trend due to substitution of the Na.

The total thermal conductivity κ_{total} is, in general, composed of the electronic and phononic part: $\kappa_{total} = \kappa_{el} + \kappa_{ph}$. If we assume that only the holes contributing to the electronic conduction, the κ_{el} can be estimated by the Wiedemann-Franz law, $\kappa_{el} = L\ \sigma\ T$, where L (L = 2.443 10^{-8} W S^{-1} K^{-2}) is the Lorenz constant, σ the electrical conductivity, and T the absolute temperature. The temperature dependence of the total thermal conductivity with electronic contribution κ_{el} of the $Na_xSr_{1-x}RuO_3$ is shown in Figure 5a.

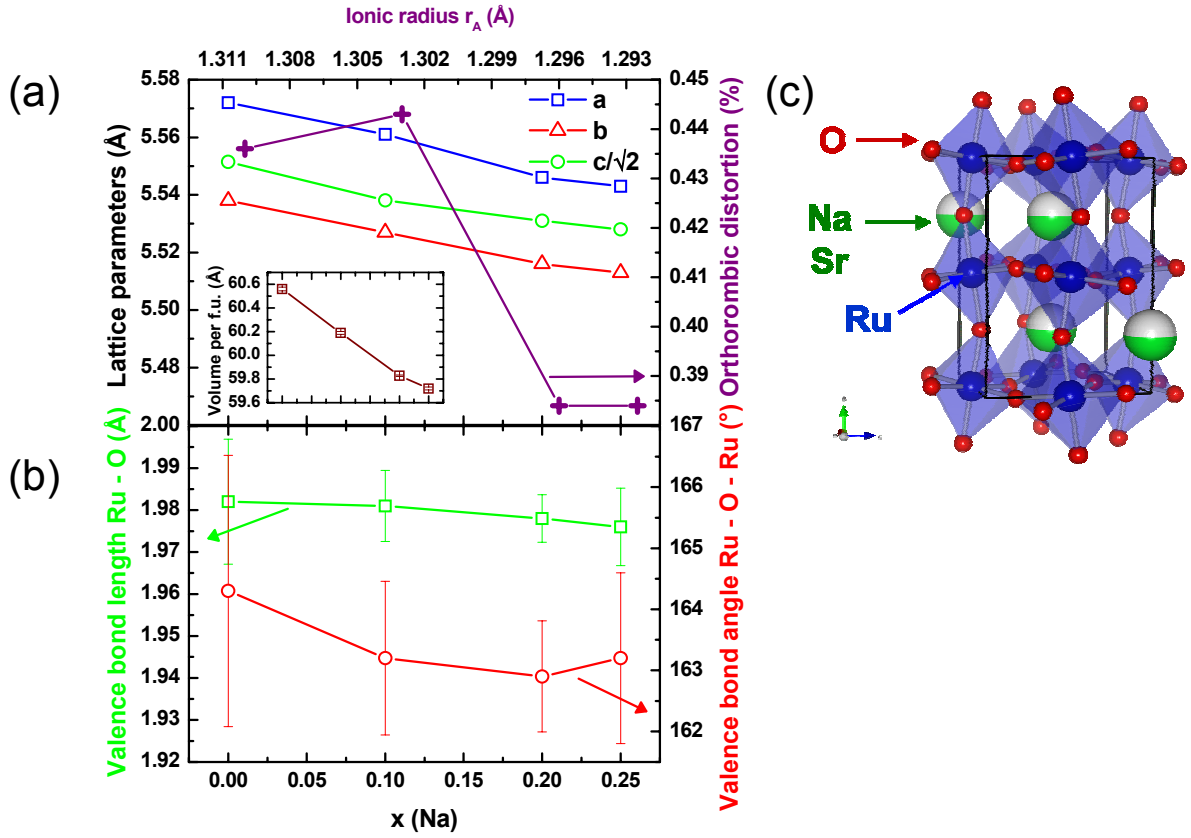

Figure 4: (a) Composition dependence of lattice parameters for $Sr_{1-x}Na_xRuO_3$ and orthorhombic distortion vs. A ionic radius for $ARuO_3$ (A = Sr, Na). The inset shows the composition dependence of the volume per f.u. (b) Composition dependence of valence bond length Ru – O and valence bond angle Ru - O - Ru. (c) Orthorhombic crystal structure of the $Sr_{0.5}Na_{0.5}RuO_3$.

The thermal conductivity increased with increasing temperature and the values are in the range between 1.5 – 2.8 W m^{-1} K^{-1}. The electronic contribution for x = 0.2 is at T = 300 K around 3 % instead for x = 0 is 21 % and for x = 0.25 it is 35 %.

The difference between κ_{total} and κ_{el}.is the phononic part, κ_{ph}. The phononic part reflects the scattering of phonons on the ground boundaries. The size of the κ_{ph} in the case of $Sr_{1-x}Na_xRuO_3$ is proportional to density of the samples. The lower density (1.49 g cm^{-3}) has sample of x = 0.25 with κ_{el} = 0.35 κ_{total} and the highest density has sample of x = 0.2 (3.32 g cm^{-3}) with κ_{el} = 0.023 κ_{total}.

Temperature dependence of the Seebeck coefficient and electrical resistivity are plotted in Figure 5b-c, respectively. All the samples show the metallic - like behaviour. The resistivity values at

300 K increased from 0.75 to 16.3 mΩ cm. Electrical resistivity values correspondence with the values of κ_{el}. Low temperature data of κ_{el} are presented in inset of Figure 5a. The highest electronic contribution of κ_{total} has the sample $Na_{0.25}Sr_{0.75}RuO_3$ with lower electrical resistivity value.

The Seebeck coefficient is positive for all samples in the whole temperature range indicating the dominant character of holes for the electronic conduction. Change of the slope of the Seebeck coefficient is observed around T_C. For the metallic system of $SrRuO_3$ below T_C the behaviour is mainly directed by the electronic correlations with linear term γ evaluated from specific heat measurements and the dimensionless ratio of 0.8, classical for metallic oxides was reported [6]. Above T_C Seebeck coefficient is less temperature dependence than below T_C and saturated between 31 – 36 μV K^{-1} around the room temperature.

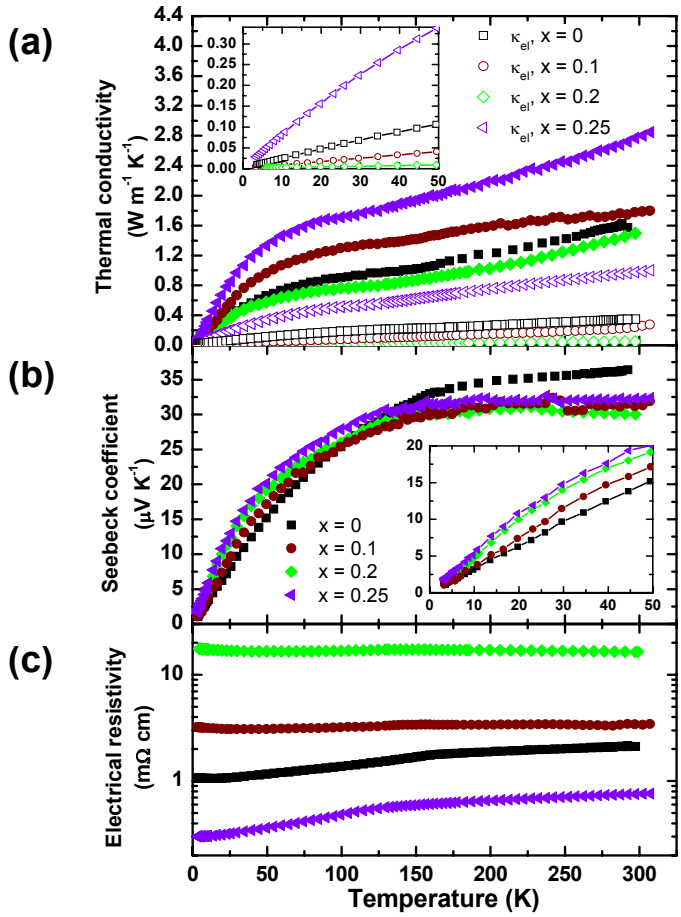

Figure 5: (a) Temperature dependence of the thermal conductivity (κ_{total}), (b) Seebeck coefficient and (c) electrical resistivity for the system $Sr_{1-x}Na_xRuO_3$ (x = 0.0 – 0.25). Closed and open symbols indicate the measured κ_{total} and estimated κ_{el}, respectively. In the inset is presented zoom up to 50 K for κ_{el}.

Temperature dependence of the molar magnetic susceptibility measured in magnetic field of 0.1 T in the temperature range from 5 K up to 400 K is plotted in Figure 6 with inset of saturated magnetic moment (M_{sat}) as function of temperature and also as dependence of Na doped amount at temperature of 5 K. The largest M_{sat} of 0.718 μ_B was observed for $SrRuO_3$ at 5 K and 0.1 T. The decreasing progress of the M_{sat} with higher concentration of Na in the samples is evident. In the inset of Figure 6 are plotted the Curie – Weiss temperature and effective magnetic moment (μ_{eff}) evaluated from the FC susceptibility curves. The FC data were fitted in paramagnetic region above T_C with Curie – Weiss

formula. The ordered effective magnetic moment is varying in the range of μ_{eff} = 2.64 μ_B for $SrRuO_3$, assuming the Landé factor g = 2, which is lower value than reported μ_{eff} = 2.81 μ_B in reference [7]. Effective magnetic moment s decreasing with increasing of Na content and creating Ru^{4+} / Ru^{5+} mixed valence. Theoretically the effective magnetic moment for $SrRuO_3$ should be μ_{eff} = 2.83 μ_B, but the measured value of 2.64 μ_B is quite close indicates that Ru^{4+} is in the low - spin state (S = 1).

Curie – Weiss temperature Θ_{CW} has positive values in all the range of Na substitution samples indicating ferromagnetism behaviour and decreasing with increasing of Na content and it is changing from 158 K for x = 0.0, which is lower value than in reference [8], up to 132 K for x = 0.25.

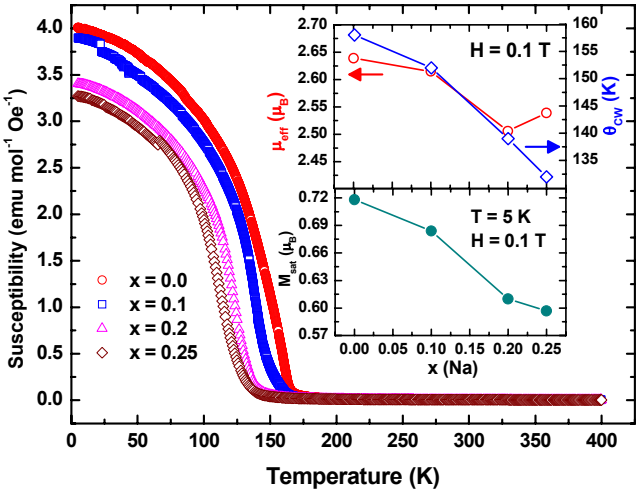

Figure 6: Temperature dependence of the molar magnetic susceptibility measured at 0.1 T on field cooling for the system $Sr_{1-x}Na_xRuO_3$ (x = 0.0 – 0.25) with the inset of saturation moments (M_{sat}) at 5 K, effective magnetic moment μ_{eff} and Curie – Weiss temperature (Θ_{CW}) for the system $Sr_{1-x}Na_xRuO_3$ (x = 0.0 – 0.25) as a function of Na doped amount.

b. **Misfit cobaltite $Ca_3Co_4O_9$**

The misfit cobaltite crystal structure contains two monoclinic subsystems, one is called rock salt type layer (RS) Ca_2CoO_3 and second one is a CoO_2 layer. The (RS) layer provides the scattering of the phonons while the CoO_2 layer ensures the conduction of the charge carriers. With this crystallographic arrangement the ZT of the material embody relatively high value among the oxide materials [9]. To understand relatively high Seebeck coefficient value of $Ca_3Co_4O_9$ [10], the specific heat Sommerfeld coefficient γ was calculated on a base of the specific heat measurement at low temperature region. The sample was measured in an applied field of H = 9 T below T = 25 K (see Figure 7b) to reduce the magnetic contribution of specific heat for more accurately evaluation of γ. Value of 85 mJ mol^{-1} K^{-2} was evaluated from the C_p / T vs. T^2 dependence (see Figure 7a) which is close to reported value by Limelette et al. [11].

Co K-edge x – ray absorption spectroscopy (XAFS) was used to determine the local structure about the Co sites. In the Figure 8 is present the zoom area around the Co – edge of XAS data measured up to 8.55 keV. To evaluate the data will be the matter of the future work.

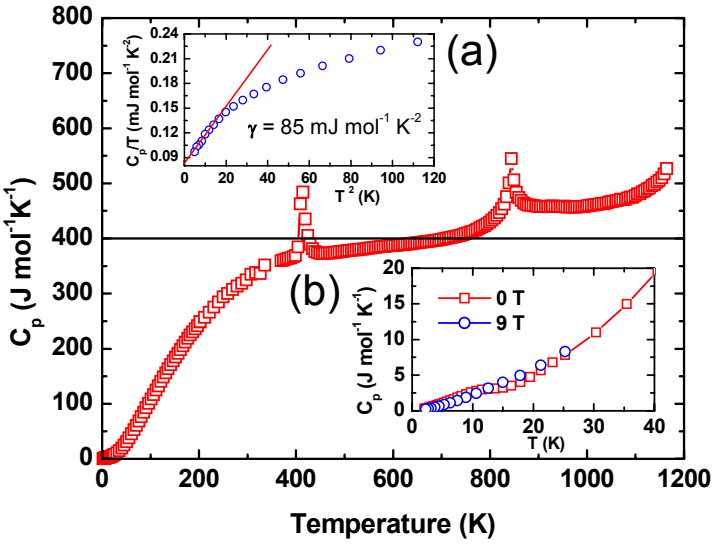

Figure 7:Temperature dependence of the specific heat for the $Ca_3Co_4O_9$ with Dulong - Petit thermodynamic limit. The inset (a) shows the low temperature specific heat measurement under H = 0 T and H = 9 T to reduce the magnetic contribution to total specific heat value and improve the evaluation of electronic part of specific heat *γ* from the C_p / T vs. T^2 dependence which is present in the inset (b).

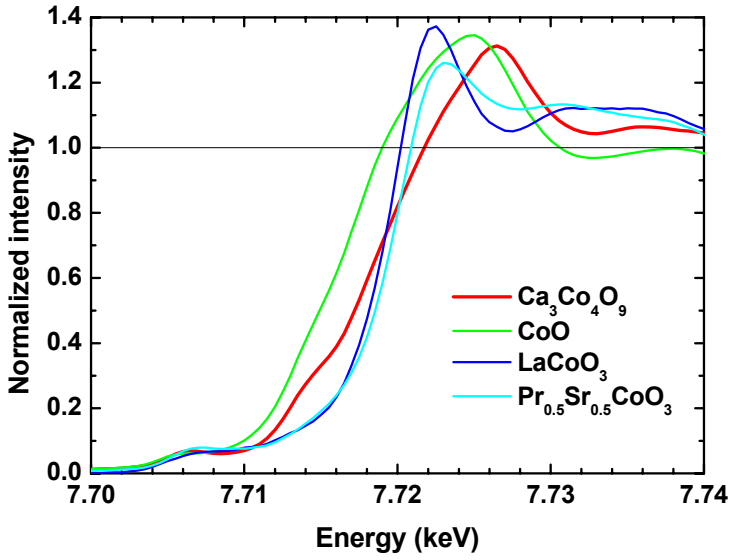

Figure 8: Normalized Co K-edges of the. $Ca_3Co_4O_9$ and the reference samples.

3) CrN – antiferromagnetic semiconductor with unusual behaviour around the Néel temperature

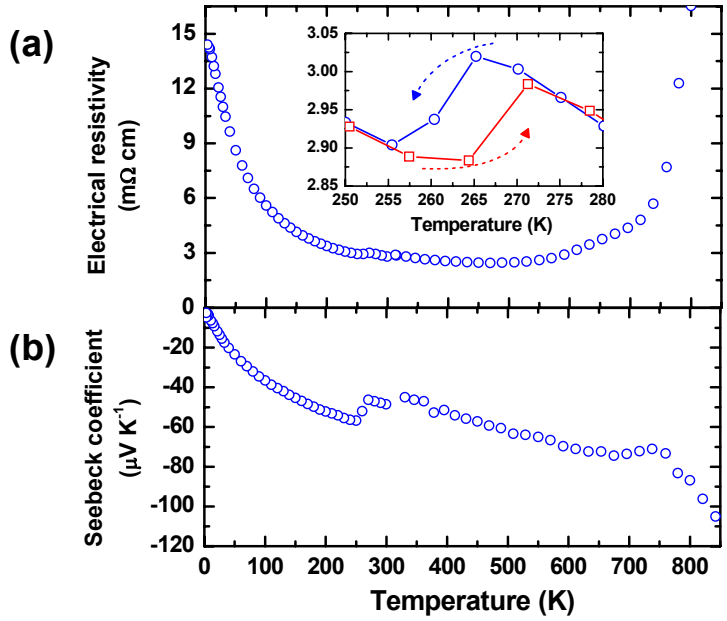

Figure 9: Temperature dependence of the (a) electrical resistivity with the zoom around T_C during the cooling and heating and (b) Seebeck coefficient for the Cr – O - N.

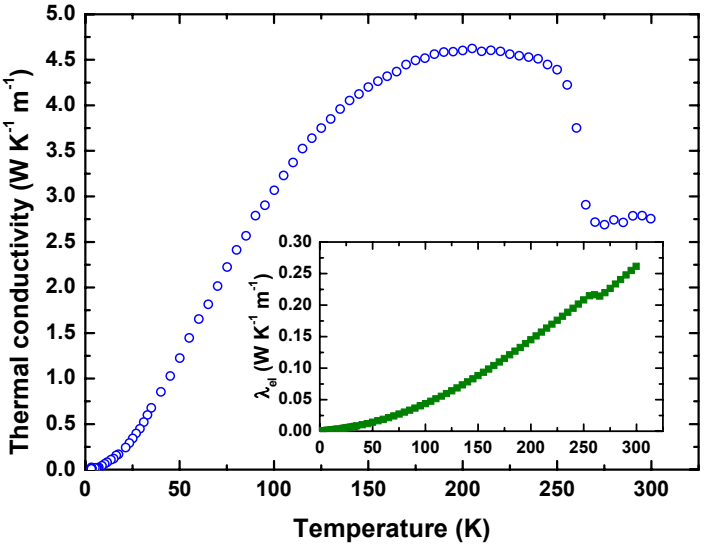

Figure 10: Temperature dependence of the thermal conductivity for the Cr – O - N. The inset present electronic contribution (λ_{el}) to total thermal conductivity.

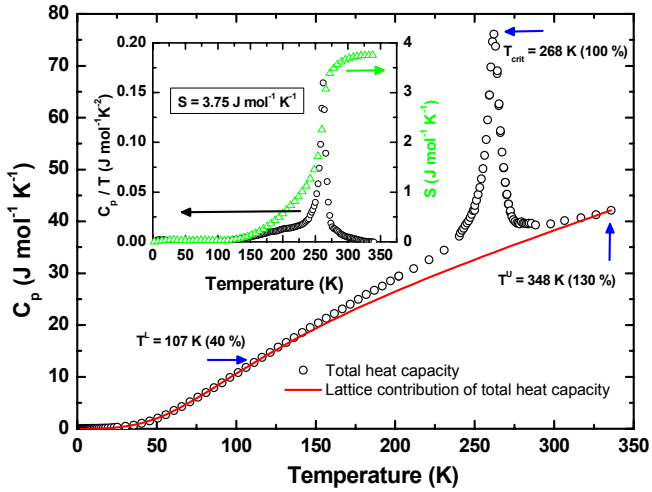

Figure 11: Temperature dependence of total heat capacity (C_p) of Cr – O - N with the function of lattice contribution of total heat capacity. The inset present temperature dependence of C_p / T and entropy (S) of phase transition.

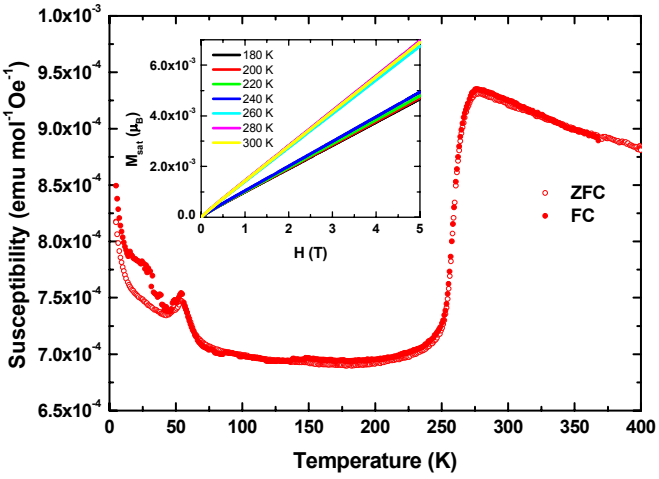

Figure 12: Temperature dependence of the molar magnetic susceptibility measured at 0.1 T on field cooling (FC) and zero field cooling (ZFC) sample for Cr – O - N with the inset of saturation moments (M_{sat}) at different temperatures in field up to 5 T.

Nationale Zusammenarbeit

- A. Bitschi, High Voltage Laboratory, Swiss Federal Institute of Technology, Physikstrasse 3, 8092 Zurich, Switzerland.
- C. Suter, Institute of Energy Technology, ETH Zurich, Sonneggstrasse 3, 8092 Zurich, Switzerland.

Internationale Zusammenarbeit

- J. Hejtmánek, Institute of Physics of ASCR, v.v.i, Laboratory of oxide materials, Na Slovance 2, 182 21 Praha 8, Czech Republic.
- E. Šantavá, Institute of Physics of ASCR, v.v.i, Department of low temperatures, Na Slovance 2, 182 21 Praha 8, Czech Republic.

Bewertung 2008 und Ausblick 2009

A four - leg thermoelectric oxide module combining *p*- and *n*-type thermoelements made of $GdCo_{0.95}Ni_{0.05}O_3$ and $CaMn_{0.98}Nb_{0.02}O_3$, respectively, was successfully used to directly convert simulated solar radiation into electrical energy using a HFSS as energy source. The TOM was tested under different ΔT ($T_h - T_c$) up to values of ΔT = 470 K. Power / voltage characteristics were evaluated under various ΔT – conditions. A maximum output power value of 0.032 W was obtained for ΔT = 450 K. From the *ZT* values of the *p*- and *n*-type materials and the measurements of the temperature on the hot and cold side of the module, a maximum conversion efficiency of ~ 1% was obtained for ΔT = 470 K.

The samples of $Sr_{1-x}Na_xRuO_3$ have an orthorhombic structure with small orthorhombic distortion which is below 1 %. The thermal conductivity increases with temperature and it is in the range of 1.5 – 2.8 W m^{-1} K^{-1} at around room temperature. The electronic contribution of thermal conductivity for x = 0.2 is around 3 % at room temperature instead for x = 0.25 it is 35 %. All the samples show the metallic - like behaviour. The Seebeck coefficient is positive for all samples in the whole temperature range and saturated between 31 – 36 μV K^{-1} for T = 300 K. M_{sat} at 5 K and 0.1 T is decreasing with higher concentration of Na. Curie – Weiss is changing from 158 K for x = 0.0 to 132 K for x = 0.25. Effective magnetic moment is changing from μ_{eff} = 2.639 μ_B for x = 0.0 up to μ_{eff} = 2.539 μ_B for x = 0.25.

Radiation aspect from the heating source as well as the radiation and the heat conduction in the module itself will be measured with the heat flux detector and compared with the theoretical calculation of C. Suter from ETH. On the base of the theoretical evaluation we will try to prepare new materials with the respect of compatibility *p*- and *n*-type material to get the maximum conversion efficiency.

To understand the origin of thermoelectricity in the promising material of $Ca_3Co_4O_9$ we will try to solve the room temperature XAS data of $Ca_3Co_4O_9$ to evaluate the crystal structure and the valence state of Co in two monoclinic subsystems and complete these data with high temperature XAS measurements in the region of spin state transition which occurs at ~ 420 K.

Referenzen

[1] R. Robert, M.H. Aguirre, P. Hug, A. Reller and A. Weidenkaff, *Acta Materiala*, Vol 55, 2007, p 4965–4972.

[2] L. Bocher, R. Robert, M. H. Aguirre, S. Malo, S. Hébert, A. Maignan. and A. Weidenkaff, *Solid State Sci.*, Vol 10, 2008, p 496-501.

[3] D. M. Rowe, Thermoelectrics handbook, 2006

[4] L. Klein, J. S. Dodge, C. H. Ahn, G. J. Snyder, T. H. Geballe, M. R. Beasley, and A. Kapitulnik, Anomalous spin scattering effects in the badly metallic itinerant ferromagnet $SrRuO_3$, Phys. Rev. Lett. 77: 13, 1996.

[5] K. Knizek, Z. Jirak, J. Hejtmanek, M. Veverka, M. Marysko, G. Maris, and T.T.M. Palstra, Structural anomalies associated with the electronic and spin transition in $LnCoO_3$, Eur. Phys. J. B, 47: 213–220, 2005.

[6] Y. Klein, S. Hebert, A. Maignan, S. Kolesnik, T. Maxwell, B. Dabrowski, Intensity of the band structure of substituted $SrRuO_3$ as probed by Seebeck coefficient measurements, Phys. Rev. B: 73: 052412, 2006.

[7] X. - Y. Zhang, Y. Chen, Z. - Y. Li, C. Vittoria and V. G. Harris, Competition between ferromagnetism and antiferromagnetism: origin of large magnetoresistance in polycrystalline $SrRu_{1-x}Mn_xO_3$ ($0 \leq x \leq 1$), J. Phys.: Condens. Matter 19: 266211, 2007.

[8] C. S. Alexander, G. Cao, S. McCall, and J. E. Crow, Magnetic and transport properties of Na doped $SrRuO_3$ and $CaRuO_3$, J. Appl. Phys., 79: 8, 1996.

[9] D. Wang, L. Chen, Q. Yao, and J. Li, High-temperature thermoelectric properties of $Ca_3Co_4O_{9+\delta}$ with Eu substitution, Solid State Commun., 129: 615-618, 2004.

[10] A. C. Masset, C. Michel, A. Maignan, M. Hervieu, O. Toulemonde, F. Studer, B. Raveau, and J. Hejtmanek, Misfit-layered cobaltite with an anisotropic giant magnetoresistance: $Ca_3Co_4O_9$, Phys. Rev. B **62** : 166, 2000.

[11] P. Limelette, V. Hardy, P. Auban-Senzier, D. Jérome, D. Flahaut, S. Hébert, R. Frésard, Ch. Simon,J. Noudem, and A. Maignan, Strongly correlated properties of the thermoelectric cobalt oxide $Ca_3Co_4O_9$, Phys. Rev. B: 71: 233108, 2005.

List of conference contributions and scientific publications in the 2008 funding period

- "First full perovskite type oxide thermoelectric module" P. Tomeš, M. Trottmann, L. Bocher, R. Robert, E. Hack, S. Toggweiler, A. Bitschi, J. Hejtmánek, A. Weidenkaff, Materials Science and Technology Conference (MS&T), Pittsburgh, 2008.
- "Full perovskite type oxide thermoelectric module" P. Tomeš, L. Bocher, R. Robert, M. H. Aguirre, M. Trottmann, and A. Weidenkaff, European Materials Research Society, Strasbourg, 2008.
- "Evaluation and power generation of *p*-type $GdCo_{0.95}Ni_{0.05}O_3$ / *n*-type $CaMn_{0.98}Nb_{0.02}O_3$ thermoelectric oxide modules (TOM)" P. Tomeš, M. Trottmann, A. Bitschi, S. Toggweiler, E. Hack, L. Bocher, R. Robert, M. H. Aguirre, D. Logvinovich, A. Shkabko and A. Weidenkaff, Swiss Physical Society meeting,Geneva, 2008.
- "Thermoelectric oxide modules for electrical power generation from solar heat" P. Tomeš, M. Trottmann, S. Toggweiler, A. Haemmerli, A. Weidenkaff, 7th Empa – PSI Ph.D. students day, Duebendorf, 2008.
- "Application and development of thermoelectric materials" P. Tomeš, M. Trottmann, R. Robert, L. Bocher, M. H. Aguirre, A. Weidenkaff, 8th Empa – PSI Ph.D. students day, Villigen, 2008.
- "Thermoelectric and magnetic properties of $Sr_{1-x}Na_xRuO_3$ (x = 0.0 – 0.25) at low temperatures (T < 300 K)" P. Tomeš, J. Hejtmánek, K. Knížek, R. Robert, L. Bocher, A. Weidenkaff, Empa PhD students day, Duebendorf, 2008.
- "Direct conversion of simulated solar radiation into electrical energy by a perovskite thermoelectric oxide module (TOM)", P. Tomeš, R. Robert, L. Bocher, M. Trottmann, M. H. Aguirre, A. Weidenkaff, P. Haueter, A. Steinfeld, J. Hejtmánek, Thermoelectric materials: Science, Technology, and Applications, Materials Science and Technology (MS&T) 2008.

Anhang